Deep Latent Graph Matching

Tianshu Yu [1] **Runzhong Wang** [2] **Junchi Yan** [2] **Baoxin Li** [1]

Abstract

Deep learning for graph matching (GM) has emerged as an important research topic due to its superior performance over traditional methods and insights it provides for solving other combinatorial problems on graph. While recent deep methods for GM extensively investigated effective node/edge *feature learning* or downstream *GM solvers* given such learned features, there is little existing work questioning if the *fixed* connectivity/topology typically constructed using heuristics (e.g., Delaunay or k-nearest) is indeed suitable for GM. From a learning perspective, we argue that the fixed topology may restrict the model capacity and thus potentially hinder the performance. To address this, we propose to learn the (distribution of) latent topology, which can better support the downstream GM task. We devise two latent graph generation procedures, one deterministic and one generative. Particularly, the generative procedure emphasizes the across-graph consistency and thus can be viewed as a matching-guided co-generative model. Our methods deliver superior performance over previous state-of-the-arts on public benchmarks, hence supporting our hypothesis.

1. Introduction

With the strong learning ability of deep networks, recent research on graph matching (GM) has migrated from traditional deterministic optimization (Schellewald & Schnörr, 2005; Cho et al., 2010; Zhou et al., 2015) towards learning-based methods (Zanfir & Sminchisescu, 2018; Wang et al., 2019; Yu et al., 2020). GM is a classic combinatorial and NP-hard problem (Loiola et al., 2007). As the mathematical cornerstone for a series of real-world applications (e.g., image matching (Wang et al., 2018b), social mining (Chiasserini et al., 2018) and protein matching (Krissinel & Henrick, 2004)), GM has received persistent attention from the machine learning and optimization communities for many years. Formally, for two graphs with n nodes each, graph matching seeks to solve[1]:

$$\max_{\mathbf{z}} \mathbf{z}^\top \mathbf{M}\mathbf{z} \qquad \text{s.t.} \quad \mathbf{Z} \in \{0,1\}^{n\times n}, \quad \mathbf{H}\mathbf{z} = \mathbf{1} \quad (1)$$

where the affinity matrix $\mathbf{M} \in \mathbb{R}_+^{n^2\times n^2}$ encodes node (diagonal elements) and edge (off-diagonal elements) affinities/similarities and $\mathbf{z}$ is the column-wise vectorization form of the permutation matrix $\mathbf{Z}$. $\mathbf{H}$ is a selection matrix ensuring each row and column of $\mathbf{Z}$ summing to 1. $\mathbf{1}$ is a column vector filled with 1. Eq. (1) is the so-called quadratic assignment problem (QAP) (Cho et al., 2010). Maximizing Eq. (1) amounts to maximizing the sum of the similarity induced by the matching vector $\mathbf{Z}$.

Recently, deep learning based GM solvers (Zanfir & Sminchisescu, 2018; Wang et al., 2019; Yu et al., 2020; Fey et al., 2020; Rolínek et al., 2020) have enabled end-to-end training of GM on high-quality human labelled datasets (e.g., Pascal VOC (Everingham et al., 2010; Bourdev & Malik, 2009) and SPair-71k (Min et al., 2019)), which greatly improved the model capacity. Any of the aforementioned deep GM algorithms behaves as an integral framework, of which the main parts cover topology construction[2], feature extraction and differentiable GM solver. In this line of works, affinity $\mathbf{M}$ (see Eq. (1)) is not obtained beforehand, but calculated using node/edge features from some feature backbones given heuristically constructed connectivity, then fed to subsequent GM solvers. Therefore, recent investigation on deep GM frameworks typically focuses on two essential parts: 1) node/edge feature backbone (e.g., graph convolutional networks (Wang et al., 2019), channel-independent embedding (Yu et al., 2020) and SplineCNN (Fey et al., 2018)); 2) GM solvers (e.g., spectral (Zanfir & Sminchisescu, 2018), linear (Wang et al., 2019) and black-box (Pogancic et al., 2020)). In particular, since the feature backbones are variants of

[1]Arizona State University [2]Shanghai Jiao Tong University. Correspondence to: Tianshu Yu <tianshuy@asu.edu>, Baoxin Li <baoxin.li@asu.edu>.

Proceedings of the 38^{th} International Conference on Machine Learning, PMLR 139, 2021.

[1]Without loss of generality, we discuss graph matching under the setting of equal number of nodes without outliers. The unequal case can be readily handled by introducing extra constraints or dummy nodes. Bipartite matching and graph isomorphism are subsets of this quadratic formulation (Loiola et al., 2007).

[2]Topology in some GM problems is pre-defined and needs to be fixed, such as graph isomorphism. In this paper, we consider a more generic case where topology construction is necessary.

Graph Neural Networks, they requires initial heuristically-constructed connectivity/topology (e.g., Delaunay (Wang et al., 2019) or k-nearest (Zhang & Lee, 2019)), and the topology remains **fixed** throughout the training procedure in almost all the existing deep GM methods. In this sense, *the construction of graph topology is only a pre-processing step, independent of the GM task*. This fixed mechanism was adopted in many GM applications ranging from computer vision (Wang et al., 2019; Yu et al., 2020; Fey et al., 2020; Rolínek et al., 2020) to social networks (Zhang & Tong, 2016; Heimann et al., 2018; Xiong & Yan, 2020).

From a learning perspective, we argue that freezing the graph topology for matching can hinder the capacity of deep GM frameworks. For a pre-defined graph topology, the linked nodes sometimes result in less meaningful or even misleading interaction. See schematic demonstrations in Fig. 1 and Fig. 5. Though some earlier attempts (Cho & Lee, 2012; Cho et al., 2013) sought to adjust the graph topology under traditional learning settings, such procedures cannot be readily integrated into end-to-end deep frameworks due to the undifferentiable nature. Our method is built upon the following hypothesis:

- *There exists some latent (distribution of) discrete topology better than what is heuristically created for GM.*

Based on this, in this paper, we set out to learn the topology (or its distribution) that is more suitable for GM. We propose an end-to-end framework, termed as deep latent graph matching (**DLGM**), to jointly learn the latent graph topology and perform GM. We leverage the power of graph generative model to automatically produce graph topology from given features and their geometric relations, under two specific prior: locality and consistency. Different from generative learning on singleton graphs (Kipf & Welling, 2016; Bojchevski et al., 2018), our graph generative learning is performed in a pairwise fashion, leading to a novel matching-guided generative paradigm.

The paper makes the following contributions:

- We explore a new direction for more flexible GM by actively learning latent topology, in contrast to previous works using fixed topology as input;
- Under this setting, we propose a deterministic optimization approach to learn graph topology for matching;
- We further present a generative way to produce latent topology, which can be adapted to other problems where graph topology is the latent structure to infer;
- With minimal modification to state-of-the-art GM pipelines, our method achieves superior performance on public benchmarks.

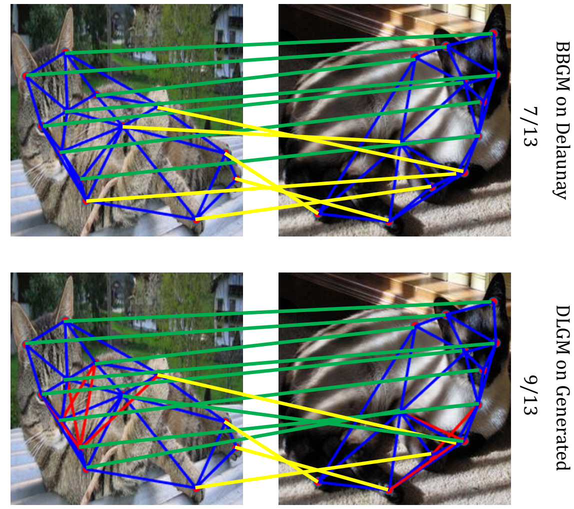

Figure 1. Matching of BBGM (Rolínek et al., 2020) 7/13 with Delaunay triangulation and our DLGM-G 9/13 using generated graph (Pascal VOC). Red edges are the ones different from blue Delaunay edges. Green and yellow lines correspond to positive and negative matchings, respectively. GM solver favors topology generated from DLGM-G, and thus leads to better accuracy.

2. Related Works

In this section, we first discuss existing works for graph topology and matching updating, whose motivation is somewhat similar to ours while the technique is largely different. Then we discuss relevant works in learning graph matching and generative graph models from the technical perspective.

Topology updating and matching. There are a few works for joint graph topology updating and matching, in the context of network alignment. Specifically, given two initial networks for matching, Du et al. (2019) showed how to alternatively perform link prediction within each network and node matching across networks based on the observation that these two tasks can benefit each other. In their extension (Du et al., 2020), a skip-gram embedding framework was further established under the same setting. These works involve random-walk-based node embedding updating and classification-based link prediction, and the whole algorithm runs in a one-shot optimization fashion. There is neither explicit training dataset nor trained matching model (except for the link classifier), which bears less flavor of machine learning. In contrast, our method involves training an explicit model for topology recovery and matching solving. Specifically, our deterministic technique (see Sec. 3.4.1) solves graph topology and matching in one-shot, while the proposed generative method alternatively estimates the topology and matching (see Sec. 3.4.2). Our approach allows the algorithm to fully leverage multiple training samples to boost the performance on the test set.

Moreover, the combinatorial nature of the matching problem is not addressed in (Du et al., 2019; 2020), where a greedy selection strategy was adopted instead. In contrast, we develop a principled combinatorial learning approach to this challenge. Also their methods rely on a considerable amount of seed matchings, yet this paper directly learns the latent topology from scratch which is more challenging and practical but yet seldom studied.

Learning of graph matching. Early shallow models sought to learn effective metric (e.g. weighted Euclid distance) for node and edge features or affinity kernel (e.g. Gaussian kernel) in a parametric fashion (Caetano et al., 2009; Cho et al., 2013). Recent deep graph matching methods have shown how to extract more dedicated features. The work (Zanfir & Sminchisescu, 2018) adopts VGG16 (Simonyan & Zisserman, 2014) as the backbone for feature extraction on images. Other efforts have been devoted to developing more advanced pipelines, where graph embedding (Wang et al., 2019; Yu et al., 2020; Fey et al., 2020) and geometric learning (Zhang & Lee, 2019; Fey et al., 2020) are involved. Rolínek et al. (2020) studied the way of incorporating traditional non-differentiable combinatorial solvers by introducing a differentiatiable blackbox GM solver (Pogancic et al., 2020). Recent works in tackling combinatorial problem with deep learning (Huang et al., 2019; Kool & Welling, 2018) also inspired development of combinatorial deep solvers for GM problems formulated by both Koopmans-Beckmann's QAP (Nowak et al., 2018; Wang et al., 2019) and Lawler's QAP (Wang et al., 2021). Specifically, Wang et al. (2019) devised a permutation loss for supervised learning, with an improvement in (Yu et al., 2020) via Hungarian attention. Wang et al. (2021) solved the most general Lawler's QAP with a graph embedding technique.

Generative graph model. Early generative models for graph can be dated back to (Erdos & Renyi, 1959), in which edges are generated with fixed probability. Recently, Kipf & Welling (2016) presented a graph generative model by re-parameterizing the edge probability from Gaussian noise. Johnson (2017) proposed to generate graph in an incremental fashion, and in each iteration a portion of the graph is produced. Gómez-Bombarelli et al. (2018) utilized recurrent neural network to generate graph from a sequence of molecule representation. Adversarial graph generation was considered in (Pan et al., 2018; Wang et al., 2018a; Bojchevski et al., 2018). Specifically, Wang et al. (2018a); Bojchevski et al. (2018) sought to unify graph generative model and generative adversarial networks. In parallel, reinforcement learning has been adopted to generate discrete graphs (De Cao & Kipf, 2018).

3. Learning Latent Topology for GM

In this section, we describe details of the proposed framework with two specific algorithms derived from *deterministic* and *generative* perspectives, respectively. Both algorithms are motivated by the *hypothesis* that there exists some latent topology more suitable for matching rather than a fixed one. Note that the proposed deterministic algorithm performs a standard forward-backward pass to jointly learn the topology and matching, while our generative algorithm consists of an alternative optimization procedure between estimating latent topology and learning matching under an Expectation-Maximization (EM) interpretation. In general, the generative algorithm assumes that a latent topology is sampled from a *latent distribution*, where the expected matching accuracy under this distribution is maximized. Therefore, we expect to learn a topology generator under such distribution. We reformulate GM in a Bayesian fashion for consistent discussion in Sec. 3.1, detail deterministic/generative latent module in Sec. 3.2 and discuss the loss functions from a probabilistic perspective in Sec. 3.3. We finally elaborate on the holistic framework and the optimization procedure for both algorithms (deterministic and generative) in Sec. 3.4.

3.1. Problem Definition and Background

Learning-based GM problem can be viewed as an extension to Eq. (1). Let $\mathcal{G}^{(s)}$ and $\mathcal{G}^{(t)}$ represent respectively the source and target graphs for matching. We represent a graph as $\mathcal{G} := \{\mathbf{X}, \mathbf{E}, \mathbf{A}\}$, where $\mathbf{X} \in \mathbb{R}^{n \times d_1}$ is the representation of n nodes with dimension d_1. $\mathbf{E} \in \mathbb{R}^{m \times d_2}$ are d_2-dimensional features of m edges and $\mathbf{A} \in \{0,1\}^{n \times n}$ is initial connectivity (i.e., topology) matrix by heuristics (e.g., Delaunay triangulation). For notational brevity, we assume d_1 and d_2 remain intact after updating the features across each convolutional layers of GNN (i.e., feature dimensions of both nodes and edges will not change after each layer's update). Denote the matching $\mathbf{Z} \in \{0,1\}^{n \times n}$ between two graphs, where $\mathbf{Z}_{ij} = 1$ indicates a correspondence exists between node i in $\mathcal{G}^{(s)}$ and node j in $\mathcal{G}^{(t)}$, and $\mathbf{Z}_{ij} = 0$ otherwise. Given training samples $\{\mathbf{Z}_k, \mathcal{G}_k^{(s)}, \mathcal{G}_k^{(t)}\}$ with $k = 1, 2, ..., N$, the objective of learning-based GM aims to maximize the likelihood:

$$\max_{\theta} \prod_{k} P_\theta \left(\mathbf{Z}_k | \mathcal{G}_k^{(s)}, \mathcal{G}_k^{(t)} \right) \tag{2}$$

where θ denotes model parameters. $P_\theta(\cdot)$ measures the probability of matching $\mathbf{Z}_k$ given the k-th pair, and is instantiated via a network parameterized by θ.

Being a generic module for producing latent topology, *our method can be flexibly and easily integrated into existing deep GM frameworks*. We build up our method based on state-of-the-art (Rolínek et al., 2020), which utilizes SplineCNN (Fey et al., 2018) for node/edge feature learning and black-box GM solver (Pogancic et al., 2020). SplineCNN is a specific graph neural networks which updates a node representation via a weighted summation of its neighbors. The update rule at node i of a standard SplineCNN reads:

$$(\mathbf{x} * \mathbf{g})(i) = \frac{1}{|\mathcal{N}(i)|} \sum_{l=1}^{d_1} \sum_{j \in \mathcal{N}(i)} x_l(j) \cdot g_l(\mathbf{e}(i,j)) \tag{3}$$

where $x_l(j)$ performs the convolution on node j and outputs a d_1-dimensional feature. $g_l(\cdot)$ delivers the message weight given the edge feature $\mathbf{e}(i,j)$. $\mathcal{N}(i)$ refers to i's neighboring nodes. Summation over neighbors follows the topology $\mathbf{A}$. Since our algorithm learns to generate topology, we need to explicitly express Eq. (3) in a differentiable way w.r.t. $\mathbf{A}$. To this end, we rewrite Eq. (3) as:

$$(\mathbf{x} * \mathbf{g} | \mathbf{A}) = (\hat{\mathbf{A}} \circ \mathbf{G})\hat{\mathbf{X}} \tag{4}$$

where $\hat{\mathbf{A}}$ is the normalized connectivity with each row normalized by the degree $|\mathcal{N}(i)|$ (see Eq. (3)) of the corresponding node i. $\mathbf{G}$ and $\hat{\mathbf{X}}$ correspond to outputs of $g_l(\cdot)$ and $x_l(\cdot)$ operators, respectively. $(\cdot \circ \cdot)$ is the Hadamard product. With Eq. (4), we thus can perform back-propagation on connectivity/topology $\mathbf{A}$. See more details in Appendix A.3.

3.2. Latent Topology Learning

Existing learning-based graph matching algorithms consider $\mathbf{A}$ to be fixed throughout the computation without questioning if the input topology is optimal or not. This can be problematic since input graph construction is heuristic, and it never takes into account how suitable it is for the subsequent GM task. In our framework, instead of utilizing a fixed pre-defined topology, we consider to produce latent topology under two settings: 1) a deterministic and 2) a generative way. The former is often more efficient while the latter method can be more accurate at the cost of exploring more latent topology. Note that both methods produce *discrete topology* to verify our hypothesis about the existence of more suitable discrete latent topology for GM. The corresponding two deep structures are described below.

Deterministic learning: Given input features $\mathbf{X}$ and initial topology $\mathbf{A}$, the deterministic way of generating latent topology $\underline{\mathbf{A}} \in \{0,1\}^{n \times n}$ is[3]:

$$\begin{aligned} \underline{\mathbf{A}}_{ij} &= \mathrm{Rounding}(\mathrm{sigmoid}(\mathbf{y}_i^\top \mathbf{W} \mathbf{y}_j)) \\ \text{with} \quad \mathbf{Y} &= \mathrm{GCN}(\mathbf{X}, \mathbf{A}) \end{aligned} \tag{5}$$

where $\mathrm{GCN}(\cdot)$ is the graph convolutional networks (GCN) (Kipf & Welling, 2017) and $\mathbf{y}_i$ corresponds to the feature of node i in feature map $\mathbf{Y}$. $\mathbf{W}$ is the learnable parameter matrix. Note that function $\mathrm{Rounding}(\cdot)$ is undifferentiable, and will be discussed in Sec. 3.4.1.

Generative learning: We reparameterize the representation:

$$P(\mathbf{y}_i | \mathbf{X}, \mathbf{A}) = \mathcal{N}(\mathbf{y}_i | \boldsymbol{\mu}_i, \mathrm{diag}(\boldsymbol{\sigma}^2)) \tag{6}$$

with $\boldsymbol{\mu} = \mathrm{GCN}_{\boldsymbol{\mu}}(\mathbf{X}, \mathbf{A})$ and $\boldsymbol{\sigma} = \mathrm{GCN}_{\boldsymbol{\sigma}}(\mathbf{X}, \mathbf{A})$ are two GCNs producing mean and covariance. It is equivalent to sampling a random vector from i.i.d. uniform distribution $\mathbf{s} \sim \mathcal{U}(\mathbf{0}, \mathbf{1})$, then applying $\mathbf{y} = \boldsymbol{\mu} + \mathbf{s} \cdot \boldsymbol{\sigma}$, where $(\cdot)$ is element-wise product.

Similar to Eq. (5), by introducing learnable parameter $\mathbf{W}$, the generative latent topology is sampled following i.i.d. distribution over each edge (i,j):

$$\begin{aligned} P(\underline{\mathbf{A}} | \mathbf{Y}) &= \prod_i \prod_j P(\underline{\mathbf{A}}_{ij} | \mathbf{y}_i, \mathbf{y}_j) \\ \text{with} \quad P(\underline{\mathbf{A}}_{ij} = 1 | \mathbf{y}_i, \mathbf{y}_j) &= \mathrm{sigmoid}(\mathbf{y}_i^\top \mathbf{W} \mathbf{y}_j) \end{aligned} \tag{7}$$

Since $\mathrm{sigmoid}(\cdot)$ maps any input into $(0,1)$, Eq. (7) can be interpreted as the probability of sampling edge (i,j). As the sampling procedure is undifferentiable, we apply Gumbel-softmax trick (Jang et al., 2017) as another reparameterization procedure. As such, a latent graph topology $\underline{\mathbf{A}}$ can be sampled fully from distribution $P(\underline{\mathbf{A}})$ and the procedure becomes differentiable.

3.3. Loss Functions

In this section, we explain three loss functions and the underlying motivation: *matching loss*, *locality loss* and *consistency loss*. The corresponding probabilistic interpretation of each loss function can be found in Sec. 3.4.2. These functions are selectively activated in DLGM-D and DLGM-G (see Sec. 3.4). In DLGM-G, different loss functions are activated in inference and learning steps.

i) Matching loss. This common term measures how the predicted matching $\hat{\mathbf{Z}}$ diverges from ground-truth $\mathbf{Z}$. Following Rolínek et al. (2020), we adopt Hamming distance on node-wise matching:

$$\mathcal{L}_M = \mathrm{Hamming}(\hat{\mathbf{Z}}, \mathbf{Z}) \tag{8}$$

ii) Locality loss. This loss is devised to account for the general prior that the produced/learnt graph topology should advocate local connections rather than distant ones, since two nodes may have less meaningful interaction once they are too distant from each other. In this sense, locality loss serves as a ***prior*** or regularizer in GM. As shown in multiple GM methods (Yu et al., 2018; Wang et al., 2019; Fey et al., 2020), Delaunay triangulation is an effective way to deliver good locality. Therefore in our method, the locality loss is the Hamming distance between the initial topology $\mathbf{A}$

[3] We here consider the node feature $\mathbf{X}$ and topology $\mathbf{A}$. Edge feature $\mathbf{E}$ can be readily integrated as another input.

(obtained from Delaunay) and predicted topology $\underline{\mathbf{A}}$ for both the source graph and the target graph:

$$\mathcal{L}_L = \text{Hamming}(\mathbf{A}^{(s)}, \underline{\mathbf{A}}^{(s)}) + \text{Hamming}(\mathbf{A}^{(t)}, \underline{\mathbf{A}}^{(t)}) \tag{9}$$

We emphasize that the locality loss serves as a *prior* for latent graph. It focuses on advocating locality, but not reconstructing the initial Delaunay triangulation (as in Graph VAE (Kipf & Welling, 2016)).

iii) Consistency loss. One can imagine that a GM solver is likely to deliver better performance if two graphs in a training pair are similar. In particular, we anticipate the latent topology $\underline{\mathbf{A}}^{(s)}$ and $\underline{\mathbf{A}}^{(t)}$ to be isomorphic under a specific matching, since isomorphic topological structures tend to be easier to match. Driven by this consideration, we devise the consistency loss which measures the level of isomorphism between latent topology $\underline{\mathbf{A}}^{(s)}$ and $\underline{\mathbf{A}}^{(t)}$:

$$\mathcal{L}_C(\cdot|\mathbf{Z}) = |\mathbf{Z}^\top \underline{\mathbf{A}}^{(s)}\mathbf{Z} - \underline{\mathbf{A}}^{(t)}| + |\mathbf{Z}\underline{\mathbf{A}}^{(t)}\mathbf{Z}^\top - \underline{\mathbf{A}}^{(s)}| \tag{10}$$

Note that $\mathbf{Z}$ does not necessarily refer to the ground-truth, but can be any predicted matching. In this sense, latent topology $\underline{\mathbf{A}}^{(s)}$ and $\underline{\mathbf{A}}^{(t)}$ can be generated jointly given the matching $\mathbf{Z}$ as guidance. This term can also serve as a consistency prior or regularization. We give a schematic example showing the merit of introducing the consistency loss in Fig. 2(b).

3.4. Framework

A schematic diagram of our framework is given in Fig. 2(a) which consists of a singleton pipeline for processing a single image. It consists of three essential modules: a feature backbone (N_B), a latent topology module (N_G) and a feature refinement module (N_R). Specifically, module N_G corresponds to Sec. 3.2 with deterministic or generative implementations. Note that the geometric relations of keypoints provide some prior for generating topology $\underline{\mathbf{A}}$. We employ VGG16 (Simonyan & Zisserman, 2014) as N_B and feed the produced node feature $\mathbf{X}$ and edge feature $\mathbf{E}$ to N_G. N_B also produces a global feature for each image. After generating the latent topology $\underline{\mathbf{A}}$, we pass over $\mathbf{X}$ and $\mathbf{E}$ together with $\underline{\mathbf{A}}$ to N_R (SplineCNN (Fey et al., 2018)). The holistic pipeline handling pairwise graph inputs can be found in Fig. 5 in Appendix A.2, which consists of two copies of singleton pipeline processing source and target data (in a Siamese fashion), respectively. Then the outputs of two singleton pipelines are formulated into affinity matrix, followed by a differentiable Blackbox GM solver (Pogancic et al., 2020) with message-passing mechanism (Swoboda et al., 2017). Note that, if N_G is removed, the holistic pipeline with only $\mathrm{N}_B + \mathrm{N}_R$ is identical to the method in (Rolínek et al., 2020). Readers are referred to this strong baseline (Rolínek et al., 2020) for more mutual algorithmic details.

3.4.1. Optimization with **Deterministic** Latent Graph

We now show how to optimize with the deterministic latent graph module, where the topology $\underline{\mathbf{A}}$ is produced by Eq. (5). The objective of matching conditioned on the produced latent topology $\underline{\mathbf{A}}$ becomes:

$$\max \prod_k P\left(\mathbf{Z}_k|\underline{\mathbf{A}}_k^{(s)}, \underline{\mathbf{A}}_k^{(t)}, \mathcal{G}_k^{(s)}, \mathcal{G}_k^{(t)}\right) \tag{11}$$

Eq. (11) can be optimized with standard back-propagation with three loss terms activated, except for the Rounding function (see Eq. (5)), which makes the procedure undifferentiable. To address this, we use straight-through operator (Bengio et al., 2013) which performs a standard rounding during the forward pass but approximates it with the gradient of identity during the backward pass on $[0, 1]$:

$$\partial \text{Rounding}(x)/\partial x = 1 \tag{12}$$

Though there exist some unbiased gradient estimators (e.g., REINFORCE (Williams, 1992)), the biased straight-through estimator proved to be more efficient and has been successfully applied in several applications (Chung et al., 2017; Campos et al., 2018). All the network modules ($\mathrm{N}_G + \mathrm{N}_B + \mathrm{N}_R$) are simultaneously learned during the training. All three losses are activated in the learning procedure (see Sec. 3.3), which are applied on the predicted matching $\hat{\mathbf{Z}}$, the latent topology $\underline{\mathbf{A}}^{(s)}$ and $\underline{\mathbf{A}}^{(t)}$. We term the algorithm under this setting **DLGM-D**.

3.4.2. Optimization with **Generative** Latent Graph

See more details in Appendix A.4. In this setting, the source and target latent topology $\underline{\mathbf{A}}^{(s)}$ and $\underline{\mathbf{A}}^{(t)}$ are *sampled* according to Eq. (6) and (7). The objective becomes:

$$\max \prod_k \int_{\underline{\mathbf{A}}_k^{(s)}, \underline{\mathbf{A}}_k^{(t)}} P_\theta\left(\mathbf{Z}_k, \underline{\mathbf{A}}_k^{(s)}, \underline{\mathbf{A}}_k^{(t)}|\mathcal{G}_k^{(s)}, \mathcal{G}_k^{(t)}\right) \tag{13}$$

Unfortunately, directly optimizing Eq. (13) is difficult due to the integration over $\underline{\mathbf{A}}$, which is intractable. Instead, we maximize the evidence lower bound (ELBO) (Bishop, 2006) as follows:

$$\begin{aligned} &\log P_\theta(\mathbf{Z}|\mathcal{G}^{(s)}, \mathcal{G}^{(t)}) \geq \\ &\mathbb{E}_{Q_\phi(\underline{\mathbf{A}}^{(s)}, \underline{\mathbf{A}}^{(t)}|\mathcal{G}^{(s)}, \mathcal{G}^{(t)})}\Big[\log P_\theta(\mathbf{Z}, \underline{\mathbf{A}}^{(s)}, \underline{\mathbf{A}}^{(t)}|\mathcal{G}^{(s)}, \mathcal{G}^{(t)}) \\ &\qquad - \log Q_\phi(\underline{\mathbf{A}}^{(s)}, \underline{\mathbf{A}}^{(t)}|\mathcal{G}^{(s)}, \mathcal{G}^{(t)})\Big] \end{aligned} \tag{14}$$

where $Q_\phi(\underline{\mathbf{A}}^{(s)}, \underline{\mathbf{A}}^{(t)}|\mathcal{G}^{(s)}, \mathcal{G}^{(t)})$ can be any joint distribution of $\underline{\mathbf{A}}^{(s)}$ and $\underline{\mathbf{A}}^{(t)}$ given the input graphs

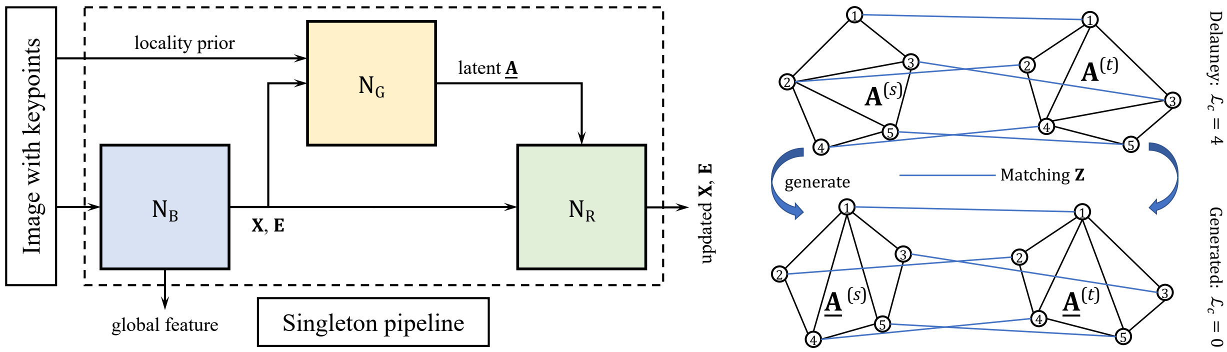

(a) Singleton pipeline of DLGM.

(b) Example of consistency loss.

Figure 2. (a) One of the two branches of our DLGM framework (see the complete version in Appendix A.2). N_B: VGG16 as backbone producing a global feature of input image, and initial $\mathbf{X}$ and $\mathbf{E}$; N_G: deterministic or generative module producing latent topology $\underline{\mathbf{A}}$; N_R: SplineCNN for feature refinement producing updated $\mathbf{X}$ and $\mathbf{E}$. (b) A schematic figure showing the merit of introducing consistency loss $\mathcal{L}_c$ for training. Initial topology $\mathbf{A}^{(s)}$ and $\mathbf{A}^{(t)}$ are constructed using Delaunay triangulation. Given matching $\mathbf{Z}$ as guidance, latent topology $\underline{\mathbf{A}}^{(s)}$ and $\underline{\mathbf{A}}^{(t)}$ are generated from inputs $\mathbf{A}^{(s)}$ and $\mathbf{A}^{(t)}$, respectively. Note that the learned topology $\underline{\mathbf{A}}^{(s)}$ and $\underline{\mathbf{A}}^{(t)}$ are isomorphic ($\mathcal{L}_c = 0$) w.r.t. $\mathbf{Z}$, which is easier to match in test, compared to non-isomorphic input structures ($\mathcal{L}_c = 4$).

$\mathcal{G}^{(s)}$ and $\mathcal{G}^{(t)}$. Equality of Eq. (14) holds when $Q_\phi(\underline{\mathbf{A}}^{(s)}, \underline{\mathbf{A}}^{(t)}|\mathcal{G}^{(s)}, \mathcal{G}^{(t)}) = P_\theta(\underline{\mathbf{A}}^{(s)}, \underline{\mathbf{A}}^{(t)}|\mathbf{Z}, \mathcal{G}^{(s)}, \mathcal{G}^{(t)})$. For tractability, we introduce the independence by assuming that we can use an identical latent topology module Q_ϕ (corresponding to N_G in Fig. 2(a)) to separately handle each input graph:

$$Q_\phi(\underline{\mathbf{A}}^{(s)}, \underline{\mathbf{A}}^{(t)}|\mathcal{G}^{(s)}, \mathcal{G}^{(t)}) = Q_\phi(\underline{\mathbf{A}}^{(s)}|\mathcal{G}^{(s)})Q_\phi(\underline{\mathbf{A}}^{(t)}|\mathcal{G}^{(t)}) \tag{15}$$

which can greatly simplify the model complexity. Then we can utilize a neural network to model Q_ϕ (similar to modeling P_θ). The optimization of Eq. (14) is studied in (Neal & Hinton, 1998), known as the Expectation-Maximization (EM) algorithm. Optimization of Eq. (14) alternates between E-step and M-step. During E-step (inference), P_θ is fixed and the algorithm seeks to find an optimal Q_ϕ to approximate the true posterior distribution (see Appendix A.4 for explanation):

$$P_\theta(\underline{\mathbf{A}}^{(s)}, \underline{\mathbf{A}}^{(t)}|\mathbf{Z}, \mathcal{G}^{(s)}, \mathcal{G}^{(t)}) \tag{16}$$

During M-step (learning), Q_ϕ is instead fixed and algorithm alters to maximize the likelihood:

$$\mathbb{E}_{Q_\phi(\underline{\mathbf{A}}^{(s)}|\mathcal{G}^{(s)}), Q_\phi(\underline{\mathbf{A}}^{(t)}|\mathcal{G}^{(t)})}\left[\log P_\theta(\mathbf{Z}, \underline{\mathbf{A}}^{(s)}, \underline{\mathbf{A}}^{(t)}|\mathcal{G}^{(s)}, \mathcal{G}^{(t)})\right] \\ \propto -\mathcal{L}_M \tag{17}$$

We detail on the inference and learning steps as follows.

Inference. This step focuses on deriving posterior distribution $P_\theta(\underline{\mathbf{A}}^{(s)}, \underline{\mathbf{A}}^{(t)}|\mathbf{Z}, \mathcal{G}^{(s)}, \mathcal{G}^{(t)})$ using its approximation Q_ϕ. To this end, we fix the parameters θ in modules N_B and N_R, and only update the parameters ϕ in module N_G corresponding to Q_ϕ. As stated in Sec. 3.2, we employ the Gumbel-softmax trick for sampling discrete $\underline{\mathbf{A}}$ (Jang et al., 2017). To this end, we can formulate a 2D vector $\mathbf{a}_{ij} = [P(\underline{\mathbf{A}}_{ij} = 1), 1 - P(\underline{\mathbf{A}}_{ij} = 1)]^\top$. Then the sampling becomes:

$$\mathrm{softmax}\left(\log(\mathbf{a}_{ij}) + \mathbf{h}_{ij}; \tau\right) \tag{18}$$

where $\mathbf{h}_{ij}$ is a random 2D vector from Gumbel distribution, and τ is a small temperature parameter. We further impose prior on latent topology $\underline{\mathbf{A}}$ given $\mathbf{A}$ through *locality loss*:

$$\log \prod_{i,j} P(\underline{\mathbf{A}}_{ij}|\mathbf{A}_{ij}) \propto -\mathcal{L}_L(\underline{\mathbf{A}}, \mathbf{A}) \tag{19}$$

which is to preserve the locality in initial topology $\mathbf{A}$. It should also be noted that $\mathbf{Z}$ is the *predicted* matching from current P_θ, as Q_ϕ is an approximation. Besides, we also anticipate two generated topology $\underline{\mathbf{A}}^{(s)}$ and $\underline{\mathbf{A}}^{(t)}$ from a graph pair should be similar (isomorphic) given $\mathbf{Z}$:

$$\log P\left(\underline{\mathbf{A}}^{(s)}, \underline{\mathbf{A}}^{(t)}|\mathbf{Z}\right) \propto -\mathcal{L}_C\left(\underline{\mathbf{A}}^{(s)}, \underline{\mathbf{A}}^{(t)}|\mathbf{Z}\right) \tag{20}$$

In summary, we activate *locality loss* and *consistency loss* as $\alpha\mathcal{L}_L + \beta\mathcal{L}_C$ during the inference step, where the latter loss is conditioned with the predicted matching rather than the ground-truth. Note that the inference step involves twice re-parameterization tricks corresponding to Eq. (6) and (18), respectively. While the first generates the continuous topology distribution under edge independence assumption, the second performs discrete sampling according to the generated topology distribution.

Learning. This step optimizes P_θ by fixing Q_ϕ. We sample discrete graph topologies $\underline{\mathbf{A}}$s completely from the probability of edge $P(\underline{\mathbf{A}}_{ij} = 1)$. Once latent topology $\underline{\mathbf{A}}$s are sampled, we feed them to module N_R together with the

Algorithm 1 DLGM-D

Input: $\mathcal{G}^s$, $\mathcal{G}^t$ and ground-truth $\mathbf{Z}$;
Output: matching $\hat{\mathbf{Z}}$;
Pretrain P_θ using Eq. (11), given Delaunay as input topology;
repeat
  # Inference (E-step):
  Obtain predicted matching $\hat{\mathbf{Z}}$ using fixed P_θ;
  Update Q_ϕ (i.e. N_G) with loss $\mathcal{L}_L + \mathcal{L}_C(\cdot|\hat{Z})$ according to Eq. (16);
  # Learning (M-step):
  Obtain predicted graph topology $\underline{\mathbf{A}}^{(s)}$ and $\underline{\mathbf{A}}^{(t)}$ using Q_ϕ;
  Update P_θ (i.e. N_B and N_R) with loss $\mathcal{L}_M$ given $\underline{\mathbf{A}}^{(s)}$ and $\underline{\mathbf{A}}^{(t)}$ according to Eq. (17);
until converge
Predict topology and the matching $\hat{\mathbf{Z}}$ with whole network activated (i.e. $\mathrm{N}_G + \mathrm{N}_B + \mathrm{N}_R$);

node-level features from N_B. Only N_B and N_R are updated in this step, and only *matching loss* $\mathcal{L}_M$ is activated.

Remark. Note for each pair of graphs in training, we use an identical random vector s for generating both graphs' topology (see Eq. (6)). We pretrain the network P_θ before alternativly training P_θ and Q_ϕ. During pretraining, we activate $\mathrm{N}_B + \mathrm{N}_R$ modules and $\mathcal{L}_M$ loss during pretraining, and feed the network the topology obtained from Delaunay as the latent topology. After pretraining, the optimization will switch between inference and learning steps until convergence. We term the setting of generative latent graph matching as **DLGM-G** and summarize it in Alg. 1.

4. Experiment

We conduct experiments on datasets including Pascal VOC with Berkeley annotation (Everingham et al., 2010; Bourdev & Malik, 2009), Willow ObjectClass (Cho et al., 2013) and SPair-71K (Min et al., 2019). We report the per-category and average performance. The objective of all experiments is to maximize the average matching accuracy. Both our **DLGM-D** and **DLGM-G** are tested. Except for the ablation study, we consistently conduct experiments under $\alpha = 5.0$ and $\beta = 0.3$. We will test different combinations of αs and βs in the ablation study (Sec. 4.4).

Peer methods. We conduct comparison experiments against the following algorithms: 1) **GMN** (Zanfir & Sminchisescu, 2018), which is a seminal work incorporating graph matching into deep learning framework equipped with a spectral solver (Egozi et al., 2012); 2) **PCA** (Wang et al., 2019). This method treats graph matching as feature matching problem and employs GCN (Kipf & Welling, 2017) to learn better features; 3) **CIE$_1$/GAT-H** (Yu et al., 2020). This paper develops an embedding and attention mechanism, where GAT-H is the version by replacing the basic embedding block with Graph Attention Networks (Veličković et al., 2018); 4) **DGMC** (Fey et al., 2020). This method devises a post-processing step by emphasizing the neighborhood similarity; 5) **BBGM** (Rolínek et al., 2020). It integrates a differentiable linear combinatorial solver (Pogancic et al., 2020) into a deep learning framework and achieves state-of-the-art performance.

4.1. Results on Pascal VOC.

This dataset (Everingham et al., 2010; Bourdev & Malik, 2009) consists of 7,020 training images and 1,682 testing images with 20 classes in total, together with the object bounding boxing for each. Following the data preparation in (Wang et al., 2019), each object within the bounding box is cropped and resized to 256×256. The number of nodes per graph ranges from 6 to 23. We further follow (Rolínek et al., 2020) under two evaluating metrics: 1) Accuracy: this is the standard metric evaluated on the keypoints by filtering out the outliers; 2) F1-score: this metric is evaluated without keypoint filtering, being the harmonic mean of precision and recall. Therefore, task 2) can be viewed as *common sub-graph matching with outliers*. Experimental results on the two setting are shown in Tab. 1 and Tab. 2. The proposed method under either settings of DLGM-D and DLGM-G outperforms counterparts by accuracy and f1-score. DLGM-G generally outperforms DLGM-D. Discussion can be found in Appendix A.5.

Quality of generated topology. We further show the consistency/locality curve vs epoch in Fig. 3, since both consistency and locality losses can somewhat reflect the quality of topology generation. It shows that both locality and consistency losses descend during the training. Note that the consistency loss with Delaunay triangulation (green dashed line) is far more larger than our generated ones (blue/red dashed line). This clearly supports the claim that our method generates similar (more isomorphic) typologies, as well as preserving locality.

4.2. Results on Willow Object.

The benchmark (Cho et al., 2013) consists of 256 images in 5 categories, where two categories (car and motorbike) are subsets from Pascal VOC. Following the protocol in Wang et al. (2019), we crop the image within the object bounding box and resize it to 256×256. Since the dataset is relatively small, we conduct the experiment to verify the transfer ability of different methods under two settings: 1) trained on Pascal VOC and directly applied to Willow (Pt); 2) trained on Pascal VOC then finetuned on Willow (Wt). Results under the two settings are shown in Tab. 4. Since this dataset is relatively small, further improvement

Table 1. Accuracy (%) on Pascal VOC (best in bold). Only inlier keypoints are considered.

METHOD	AERO	BIKE	BIRD	BOAT	BOTTLE	BUS	CAR	CAT	CHAIR	COW	TABLE	DOG	HORSE	MBIKE	PERSON	PLANT	SHEEP	SOFA	TRAIN	TV	AVE
GMN	31.1	46.2	58.2	45.9	70.6	76.4	61.2	61.7	35.5	53.7	58.9	57.5	56.9	49.3	34.1	77.5	57.1	53.6	83.2	88.6	57.9
GAT-H	47.2	61.6	63.2	53.3	79.7	70.1	65.3	70.5	38.4	64.7	62.9	65.1	66.2	62.5	41.1	78.8	67.1	61.6	81.4	91.0	64.6
PCA	40.9	55.0	65.8	47.9	76.9	77.9	63.5	67.4	33.7	65.5	63.6	61.3	68.9	62.8	44.9	77.5	67.4	57.5	86.7	90.9	63.8
CIE_1-H	51.2	69.2	70.1	55.0	82.8	72.8	69.0	74.2	39.6	68.8	71.8	70.0	71.8	66.8	44.8	85.2	69.9	65.4	85.2	92.4	68.9
DGMC	50.4	67.6	70.7	70.5	87.2	85.2	82.5	74.3	46.2	69.4	69.9	73.9	73.8	65.4	51.6	98.0	73.2	69.6	94.3	89.6	73.2
BBGM	61.5	75.0	78.1	80.0	87.4	93.0	89.1	80.2	58.1	77.6	76.5	79.3	78.6	78.8	66.7	97.4	76.4	77.5	**97.7**	94.4	80.1
DLGM-D (OURS)	60.8	76.0	77.5	79.6	**88.0**	**95.0**	**90.4**	81.6	67.3	82.4	**94.1**	79.6	81.2	80.5	68.9	**98.6**	77.1	87.5	97.0	95.3	82.9
DLGM-G (OURS)	**64.7**	**78.1**	**78.4**	**81.0**	87.2	94.6	89.7	**82.5**	**68.5**	**83.0**	93.9	**82.3**	**82.8**	**82.7**	**69.6**	**98.6**	**78.9**	**88.9**	97.4	**96.7**	**83.8**

Table 2. F1-score (%) on Pascal VOC. Experiment are performed on a pair of images where both inlier and outlier keypoints are considered. BBGM-max is a setting in Rolínek et al. (2020).

METHOD	AERO	BIKE	BIRD	BOAT	BOTTLE	BUS	CAR	CAT	CHAIR	COW	TABLE	DOG	HORSE	MBIKE	PERSON	PLANT	SHEEP	SOFA	TRAIN	TV	AVE
BBGM-MAX	35.5	68.6	46.7	36.1	85.4	58.1	25.6	51.7	27.3	51.0	46.0	46.7	48.9	58.9	29.6	93.6	42.6	35.3	70.7	79.5	51.9
BBGM	42.7	70.9	57.5	46.6	85.8	64.1	51.0	63.8	42.4	63.7	47.9	61.5	63.4	69.0	46.1	94.2	57.4	39.0	**78.0**	82.7	61.4
DLGM-D (OURS)	42.5	71.8	57.8	46.8	**86.9**	70.3	**53.4**	66.7	53.8	67.6	64.7	64.6	65.2	70.1	**47.9**	95.5	59.6	47.7	77.7	82.6	63.9
DLGM-G (OURS)	**43.8**	**72.9**	**58.5**	**47.4**	86.4	**71.2**	53.1	**66.9**	**54.6**	**67.8**	**64.9**	**65.7**	**66.9**	**70.8**	47.4	**96.5**	**61.4**	**48.4**	77.5	**83.9**	**64.8**

Table 3. Accuracy (%) on SPair-71K compared with state-of-the-art methods (best in bold).

METHOD	AERO	BIKE	BIRD	BOAT	BOTTLE	BUS	CAR	CAT	CHAIR	COW	DOG	HORSE	MBIKE	PERSON	PLANT	SHEEP	TRAIN	TV	AVE
DGMC	54.8	44.8	80.3	70.9	65.5	90.1	78.5	66.7	66.4	73.2	66.2	66.5	65.7	59.1	98.7	68.5	84.9	98.0	72.2
BBGM	66.9	57.7	85.8	78.5	66.9	95.4	86.1	74.6	68.3	78.9	73.0	67.5	79.3	73.0	**99.1**	74.8	95.0	**98.6**	78.9
DLGM-D (OURS)	69.8	64.4	**86.8**	79.9	**69.8**	**96.8**	**87.3**	77.7	77.5	83.1	76.7	**69.6**	**85.1**	75.1	98.7	76.4	95.8	97.9	81.3
DLGM-G (OURS)	**70.4**	**66.8**	86.7	**81.7**	69.2	96.4	85.8	**79.5**	**78.4**	**84.0**	**79.4**	69.4	84.5	**76.6**	**99.1**	**75.9**	**96.4**	98.5	**82.0**

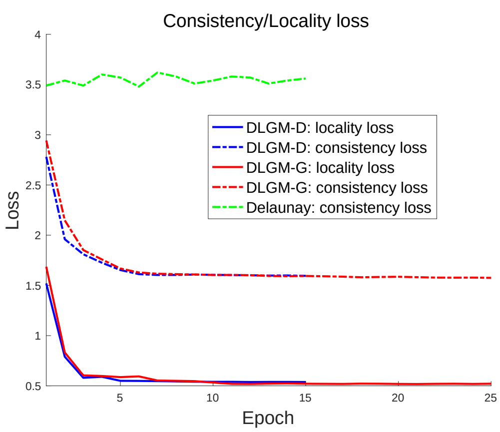

Figure 3. Consistency loss (Eq. (9) and locality loss (Eq. 10)) keep decrease over training which suggests the effectiveness for adaptive topology learning for matching.

Table 4. Accuracy (%) on Willow Object.

METHOD	SETTING	FACE	MBIKE	CAR	DUCK	WBOTTLE
GMN	PT	98.1	65.0	72.9	74.3	70.5
	WT	99.3	71.4	74.3	82.8	76.7
PCA	PT	100.0	69.8	78.6	82.4	95.1
	WT	100.0	76.7	84.0	93.5	96.9
CIE	PT	99.9	71.5	75.4	73.2	97.6
	WT	100.0	90.0	82.2	81.2	97.6
DGMC	PT	98.6	69.8	84.6	76.8	90.7
	WT	100.0	98.8	96.5	93.2	99.9
BBGM	PT	100.0	95.8	89.1	89.8	97.9
	WT	100.0	98.9	95.7	93.1	99.1
DLGM-D (OURS)	PT	100.0	95.5	91.3	91.4	97.9
	WT	100.0	99.4	95.9	92.8	99.3
DLGM-G (OURS)	PT	99.9	96.4	92.0	91.8	98.0
	WT	100.0	99.3	96.5	93.7	99.3

is difficult. It is shown both DLGM-D and DLGM-G have good transfer ability.

4.3. Results on SPair-71K.

This dataset (Min et al., 2019) is much larger than Pascal VOC and WillowObject. It consists of 70,958 image pairs collected from Pascal VOC 2012 and Pascal 3D+ (53,340 for training, 5,384 for validation and 12,234 for testing). It improves Pascal VOC by removing ambiguous categories *sofa* and *dining table*. This dataset is considered to contain more difficult matching instances and higher annotation quality. Results are summarized in Tab. 3. Our method consistently improves the matching performance, agreeing with those in Pascal VOC and Willow.

Table 5. Selectively deactivating loss functions on Pascal VOC. $\mathcal{L}_M$, $\mathcal{L}_C$ and $\mathcal{L}_L$ are selectively activated in DLGM-D and DLGM-G. "full" indicates all loss functions are activated. Average accuracy (%) is reported.

METHOD	AVE
DLGM-D ($\mathcal{L}_M + \mathcal{L}_C$)	79.8
DLGM-D ($\mathcal{L}_M + \mathcal{L}_L$)	79.5
DLGM-G ($\mathcal{L}_M + \mathcal{L}_C$)	80.9
DLGM-G ($\mathcal{L}_M + \mathcal{L}_L$)	80.4
DLGM-D (FULL)	82.9
DLGM-G (FULL)	83.8

4.4. Ablation study

We conduct ablation to show the effectiveness of some factors involved in our framework (e.g., sampling size of the generator and varying loss strength α and β).

In the first part, we evaluate the performance of DLGM-D and DLGM-G by selectively deactivating different loss functions $\mathcal{L}_M$, $\mathcal{L}_C$ and $\mathcal{L}_L$. Since our method involves a sampling procedure, we also conduct the test on DLGM-G using different sample size of the generator. This ablation test is conducted on Pascal VOC dataset and average accuracy is reported in Tab. 5 and 6.

We first test the performance of both settings of DLGM by selectively activate the designated loss functions. Experimental results are summarized in Tab. 5. As matching loss $\mathcal{L}_M$ is essential for GM task, we constantly activate this loss for all settings. Note once $\mathcal{L}_C$ and $\mathcal{L}_L$ are both deactivated, our method will degenerate into BBGM (Rolínek et al., 2020). In this case, there will be no need to train the generator Q_ϕ. We see that the proposed novel losses $\mathcal{L}_C$ and $\mathcal{L}_L$ can consistently enhance the matching performance. Besides, DLGM-G indeed delivers better performance than DLGM-D under fair comparison.

We then test the impact of sample size from the generator Q_ϕ under DLGM-G. Experimental results are summarized in Tab. 6. We see that along with the increasing sample size, the average accuracy ascends. The performance becomes stable when the sample size reaches over 16.

Remark. In terms of the time efficiency, if we consider the training time of the baseline (Rolínek et al., 2020) to be 1x, the training time of our method under discriminative setting is around 1.2x-1.3x. The time cost of our method under generative setting is around 8x-9x with sample size 16. We didn't observe any obvious efficiency gap for the testing stage.

In the second part, we present more detailed results by varying the loss strength αs and βs for DLGM-G. Letting the loss at inference step be $\alpha\mathcal{L}_L + \beta\mathcal{L}_C$, Tab. 7 shows the performance of DLGM-G with varying α and β on Pascal VOC with only inliers (Note we reported $\alpha = 5.0$ and $\beta = 0.3$ in all the previous experiments on each dataset):

Table 6. Average matching accuracy under different sampling sizes from the generator Q_ϕ with "full" DLGM-G setting.

#SAMPLE	AVE
1	82.5
2	83.2
4	83.2
8	83.5
16	83.8
32	83.7

Table 7. Ablation study of DLGM-G on Pascal VOC dataset. α and β correspond to the strength of locality loss $\mathcal{L}_L$ and consistency loss $\mathcal{L}_C$, respectively. Average accuracy (%) is reported.

α \ β	0.1	0.2	0.3	0.4	0.5
4.0	82.0	81.8	82.4	82.1	81.9
4.5	82.2	82.6	82.9	82.5	82.5
5.0	82.3	83.3	83.8	83.1	82.5
5.5	82.0	82.9	83.3	83.0	82.7

5. Conclusion

Recent deep GM methods have delivered significant performance gain over traditional ones through learning node/edge features and GM solvers. However, beyond relying on heuristics, there is little work on learning more effective topology for improved matching. In this paper, we hypothesize that learning a better (distribution of) discrete graph topology can significantly improve the matching, thus being essential. As such, we propose to incorporate a latent topology module under an end-to-end deep framework that learns to produce better graph topology. We present the interpretation and optimization of the topology learning module from deterministic and generative perspectives respectively. Experimental results show that, by learning the latent topology, the matching performance can be consistently and significantly enhanced on several public datasets, with only minimal modification to existing method.

Acknowledgements

This work was supported in part by a grant from ONR. Any opinions expressed in this material are those of the authors and do not necessarily reflect the views of ONR.

References

Bengio, Y., Léonard, N., and Courville, A. Estimating or propagating gradients through stochastic neurons for conditional computation. *arXiv preprint arXiv:1308.3432*, 2013.

Bishop, C. M. *Pattern recognition and machine learning*. springer, 2006.

Bojchevski, A., Shchur, O., Zügner, D., and Günnemann, S. Netgan: Generating graphs via random walks. In *ICML*, 2018.

Bourdev, L. and Malik, J. Poselets: Body part detectors trained using 3d human pose annotations. In *ICCV*, 2009.

Caetano, T., McAuley, J., Cheng, L., Le, Q., and Smola, A. J. Learning graph matching. *TPAMI*, 31(6):1048–1058, 2009.

Campos, V., Jou, B., Giró-i Nieto, X., Torres, J., and Chang, S.-F. Skip rnn: Learning to skip state updates in recurrent neural networks. In *ICLR*, 2018.

Chiasserini, C.-F., Garetto, M., and Leonardi, E. De-anonymizing clustered social networks by percolation graph matching. *ACM Transactions on Knowledge Discovery from Data (TKDD)*, 12(2):1–39, 2018.

Cho, M. and Lee, K. M. Progressive graph matching: Making a move of graphs via probabilistic voting. In *CVPR*, 2012.

Cho, M., Lee, J., and Lee, K. M. Reweighted random walks for graph matching. In *ECCV*, 2010.

Cho, M., Alahari, K., and Ponce, J. Learning graphs to match. In *ICCV*, 2013.

Chung, J., Ahn, S., and Bengio, Y. Hierarchical multiscale recurrent neural networks. In *ICLR*, 2017.

De Cao, N. and Kipf, T. Molgan: An implicit generative model for small molecular graphs. *arXiv preprint arXiv:1805.11973*, 2018.

Du, X., Yan, J., and Zha, H. Joint link prediction and network alignment via cross-graph embedding. *IJCAI*, 2019.

Du, X., Yan, J., Zhang, R., and Zha, H. Cross-network skip-gram embedding for joint network alignment and link prediction. *IEEE Transactions on Knowledge and Data Engineering*, 2020.

Egozi, A., Keller, Y., and Guterman, H. A probabilistic approach to spectral graph matching. *TPAMI*, 35(1):18–27, 2012.

Erdos, P. and Renyi, A. On random graphs i. In *Publicationes Mathematicae Debrecen 6*, 1959.

Everingham, M., Gool, L., Williams, C. K., Winn, J., and Zisserman, A. The pascal visual object classes (voc) challenge. *Int. J. Comput. Vision*, 88(2):303–338, June 2010.

Fey, M., Eric Lenssen, J., Weichert, F., and Müller, H. Splinecnn: Fast geometric deep learning with continuous b-spline kernels. In *CVPR*, 2018.

Fey, M., Lenssen, J. E., Morris, C., Masci, J., and Kriege, N. M. Deep graph matching consensus. In *ICLR*, 2020.

Gómez-Bombarelli, R., Wei, J. N., Duvenaud, D., Hernández-Lobato, J. M., Sánchez-Lengeling, B., Sheberla, D., Aguilera-Iparraguirre, J., Hirzel, T. D., Adams, R. P., and Aspuru-Guzik, A. Automatic chemical design using a data-driven continuous representation of molecules. *ACS central science*, 4(2):268–276, 2018.

Heimann, M., Shen, H., Safavi, T., and Koutra, D. Regal: Representation learning-based graph alignment. In *CIKM*, 2018.

Huang, J., Patwary, M., and Diamos, G. Coloring big graphs with alphagozero. *arXiv:1902.10162*, 2019.

Jang, E., Gu, S., and Poole, B. Categorical reparameterization with gumbel-softmax. In *ICLR*, 2017.

Johnson, D. D. Learning graphical state transitions. In *ICLR*, 2017.

Kipf, T. N. and Welling, M. Variational graph auto-encoders. *arXiv preprint arXiv:1611.07308*, 2016.

Kipf, T. N. and Welling, M. Semi-supervised classification with graph convolutional networks. In *ICLR*, 2017.

Kool, W. and Welling, M. Attention solves your tsp. *arXiv:1803.08475*, 2018.

Krissinel, E. and Henrick, K. Secondary-structure matching (ssm), a new tool for fast protein structure alignment in three dimensions. *Acta Crystallographica Section D: Biological Crystallography*, 60(12):2256–2268, 2004.

Loiola, E. M., de Abreu, N. M., Boaventura-Netto, P. O., Hahn, P., and Querido, T. A survey for the quadratic assignment problem. *EJOR*, pp. 657–90, 2007.

Min, J., Lee, J., Ponce, J., and Cho, M. Spair-71k: A large-scale benchmark for semantic correspondence. *arXiv preprint arXiv:1908.10543*, 2019.

Neal, R. M. and Hinton, G. E. A view of the em algorithm that justifies incremental, sparse, and other variants. In *Learning in graphical models*, pp. 355–368. Springer, 1998.

Nowak, A., Villar, S., Bandeira, A., and Bruna, J. Revised note on learning quadratic assignment with graph neural networks. In *DSW*, 2018.

Pan, S., Hu, R., Long, G., Jiang, J., Yao, L., and Zhang, C. Adversarially regularized graph autoencoder for graph embedding. In *IJCAI*, 2018.

Piegl, L. and Tiller, W. *The NURBS book*. Springer Science & Business Media, 2012.

Pogancic, M. V., Paulus, A., Musil, V., Martius, G., and Rolínek, M. Differentiation of black-box combinatorial solvers. In *ICLR*, 2020.

Rolínek, M., Swoboda, P., Zietlow, D., Paulus, A., Musil, V., and Martius, G. Deep graph matching via blackbox differentiation of combinatorial solvers. In *ECCV*, 2020.

Schellewald, C. and Schnörr, C. Probabilistic subgraph matching based on convex relaxation. In *EMMCVPR*, 2005.

Simonyan, K. and Zisserman, A. Very deep convolutional networks for large-scale image recognition. In *ICLR*, 2014.

Swoboda, P., Rother, C., Abu Alhaija, H., Kainmuller, D., and Savchynskyy, B. A study of lagrangean decompositions and dual ascent solvers for graph matching. In *CVPR*, 2017.

Veličković, P., Cucurull, G., Casanova, A., Romero, A., Liò, P., and Bengio, Y. Graph Attention Networks. In *ICLR*, 2018.

Wang, H., Wang, J., Wang, J., Zhao, M., Zhang, W., Zhang, F., Xie, X., and Guo, M. Graphgan: Graph representation learning with generative adversarial nets. In *AAAI*, 2018a.

Wang, Q., Zhou, X., and Daniilidis, K. Multi-image semantic matching by mining consistent features. In *CVPR*, 2018b.

Wang, R., Yan, J., and Yang, X. Learning combinatorial embedding networks for deep graph matching. In *ICCV*, 2019.

Wang, R., Yan, J., and Yang, X. Neural graph matching network: Learning lawler's quadratic assignment problem with extension to hypergraph and multiple-graph matching. *IEEE Transactions on Pattern Analysis and Machine Intelligence*, 2021.

Williams, R. J. Simple statistical gradient-following algorithms for connectionist reinforcement learning. *Machine Learning*, 8(3):229–256, 1992.

Xiong, H. and Yan, J. Btwalk: Branching tree random walk for multi-order structured network embedding. *IEEE Transactions on Knowledge and Data Engineering*, 2020.

Yu, T., Yan, J., Wang, Y., Liu, W., et al. Generalizing graph matching beyond quadratic assignment model. In *NIPS*, 2018.

Yu, T., Wang, R., Yan, J., and Li, B. Learning deep graph matching with channel-independent embedding and hungarian attention. In *ICLR*, 2020.

Zanfir, A. and Sminchisescu, C. Deep learning of graph matching. In *CVPR*, 2018.

Zhang, S. and Tong, H. Final: Fast attributed network alignment. In *Proceedings of the 22nd ACM SIGKDD International Conference on Knowledge Discovery and Data Mining*, 2016.

Zhang, Z. and Lee, W. S. Deep graphical feature learning for the feature matching problem. In *ICCV*, 2019.

Zhou, T., Lee, Y. J., Yu, S. X., and Efros, A. A. Flowweb: Joint image set alignment by weaving consistent, pixel-wise correspondences. In *CVPR*, 2015.